

Supporting Information:

Engineering Interface-Dependent Photoconductivity in $\text{Ge}_2\text{Sb}_2\text{Te}_5$ Nanoscale Devices

Syed Ghazi Sarwat¹, Nathan Youngblood¹, Yat-Yin Au², Jan A. Mol¹, C David Wright², & Harish Bhaskaran^{1*}

harish.bhaskaran@materials.ox.ac.uk

¹Department of Materials, University of Oxford, Oxford, OX1 3PH, UK

²Department of Engineering, University of Exeter, Exeter, EX4 4QF, UK

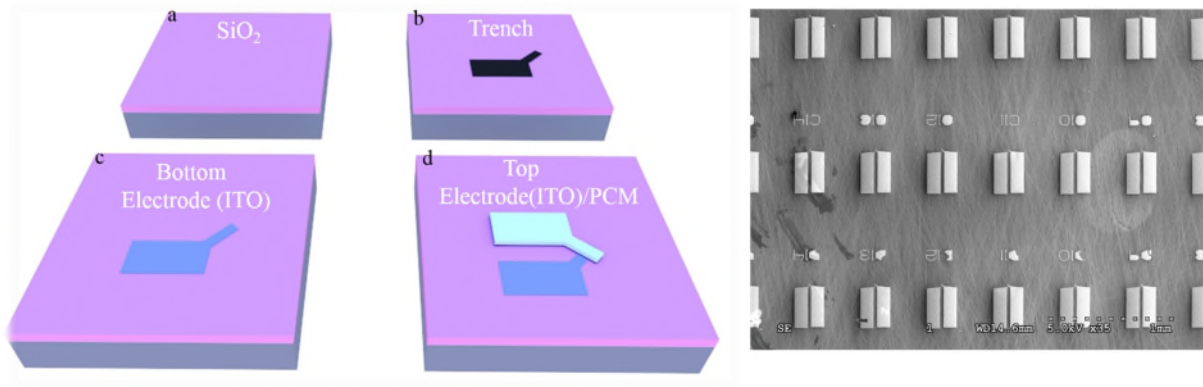


Figure S1. **Crossbar Device Fabrication.** (a) A four inch silicon wafer with 300 nm thermally grown SiO₂ passivating layer was diced into 1cm by 1 cm chips; (b) using photolithography (S1813 positive resist) top ITO electrodes were patterned on the wafer, which were subsequently used as a mask for reactive ion etching (CHF₃+Ar+O₂) to selectively etch SiO₂ into trenches (black feature); (c) using a sputtering tool Ta (10nm)/Pt(50nm)/ITO(40nm) deposition was carried-out to fill the trenches. Ta is used as an adhesive layer, Pt as mirror and ITO is the bottom electrode and (d) another photolithography step (S1813 positive resist) is executed to pattern the top electrode such that only the finger electrodes overlap with the bottom electrode, after which deposition of PCM (GST/GT) and ITO using the same sputtering under similar conditions is carried-out. A scanning electron micrograph of one of the chips is illustrated in the image on the right.

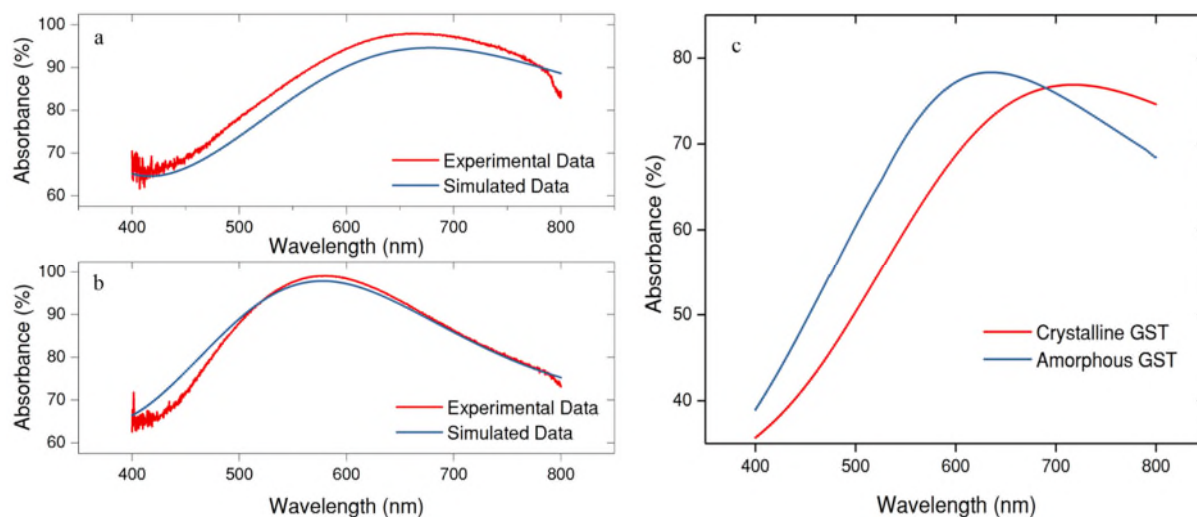


Figure S2. **Broad wavelength absorption measurements.** (a and b) Experimental (using reflectance measurements on a customized set-up, with assumption transmission is zero) and simulated measurements (using transfer matrix calculations (see Ref¹)) for the stack (Ta/Pt(50nm)/ITO (40nm)/GST(21nm)/ITO(80nm)) in the crystalline (a) and amorphous (b) state of GST. The stack shows high absorption in the visible region of the spectra in both the states of GST, and (c) from fitting using transfer matrix calculations the percentage absorption only in the GST layer is computed. The amorphous state absorbs more than crystalline state beyond till ~700 nm beyond which the crystalline state becomes more absorptive. At 637 nm wavelength where most of the measurements are made the amorphous state absorbs 5.5 % more than the crystalline counterpart.

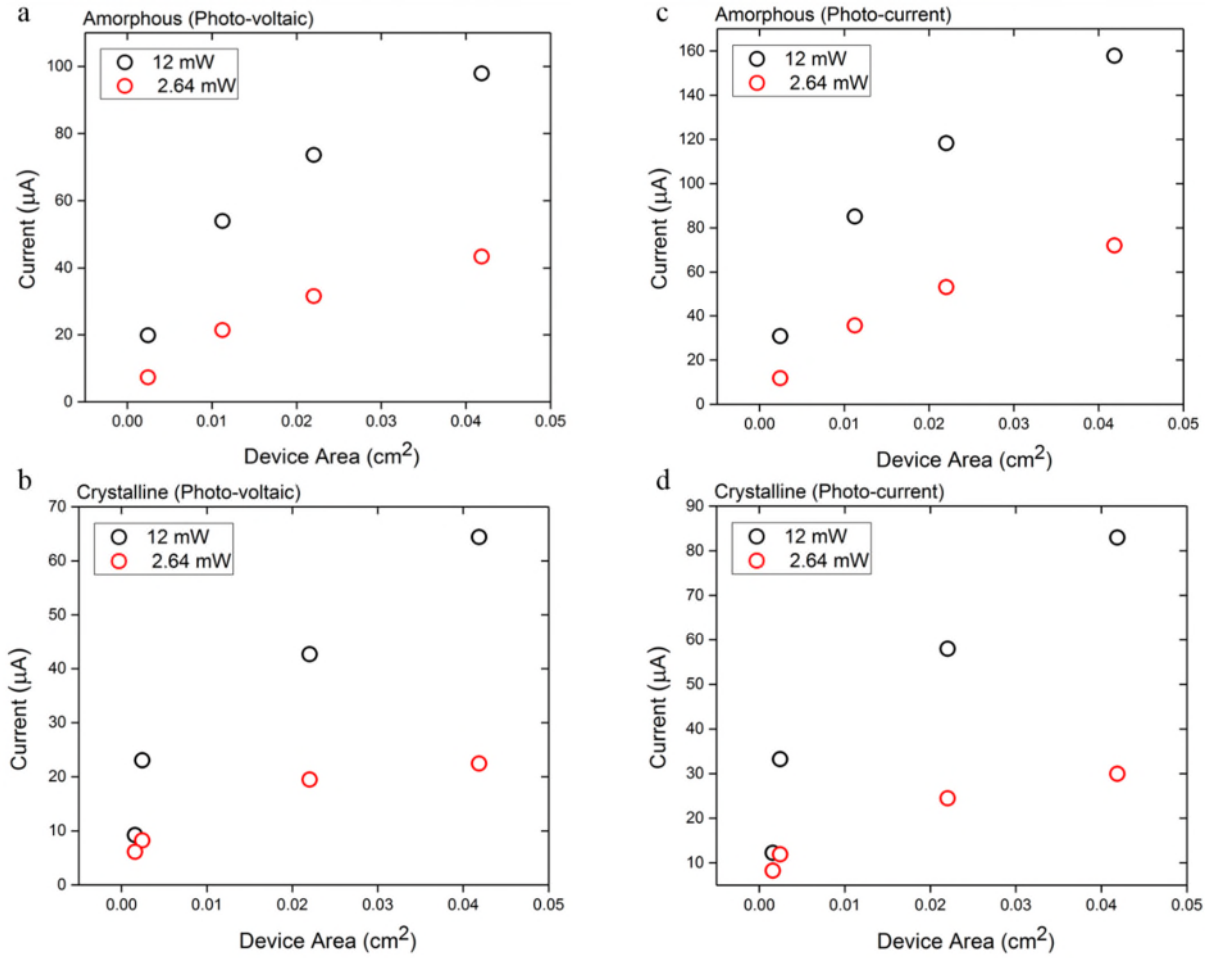


Figure S3. Scaling behaviour of the crossbar devices. (a) Photo-voltaic short-circuit current scaling as a function of the active device area in the amorphous state of GST at 12 mW and 2.64 mW exposure (637 nm) (b) photo-current current ($I_{\text{Illumination}} - I_{\text{Dark}}$) measured at 100 mV as a function of the active device area in the amorphous state of GST 12 mW and 2.64 mW exposure (637 nm); (c) photo-voltaic short-circuit current scaling as a function of the active device area in the crystalline state of GST 12 mW and 2.64 mW exposure (637 nm); and (d) photocurrent ($I_{\text{Illumination}} - I_{\text{Dark}}$) measured at 100 mV as a function of the active device area in the amorphous state of GST 12 mW and 2.64 mW exposure (637 nm). The photo-response increases with a power law dependence on the device area (fitting factor > 0.50). Note- the device is switched from the amorphous to crystalline state electrically at sub-3 V and at significantly higher currents (mA) likely due to diminished joule heating from increased thermal losses and partial crystallization of the amorphous phase from photo-induced heating.

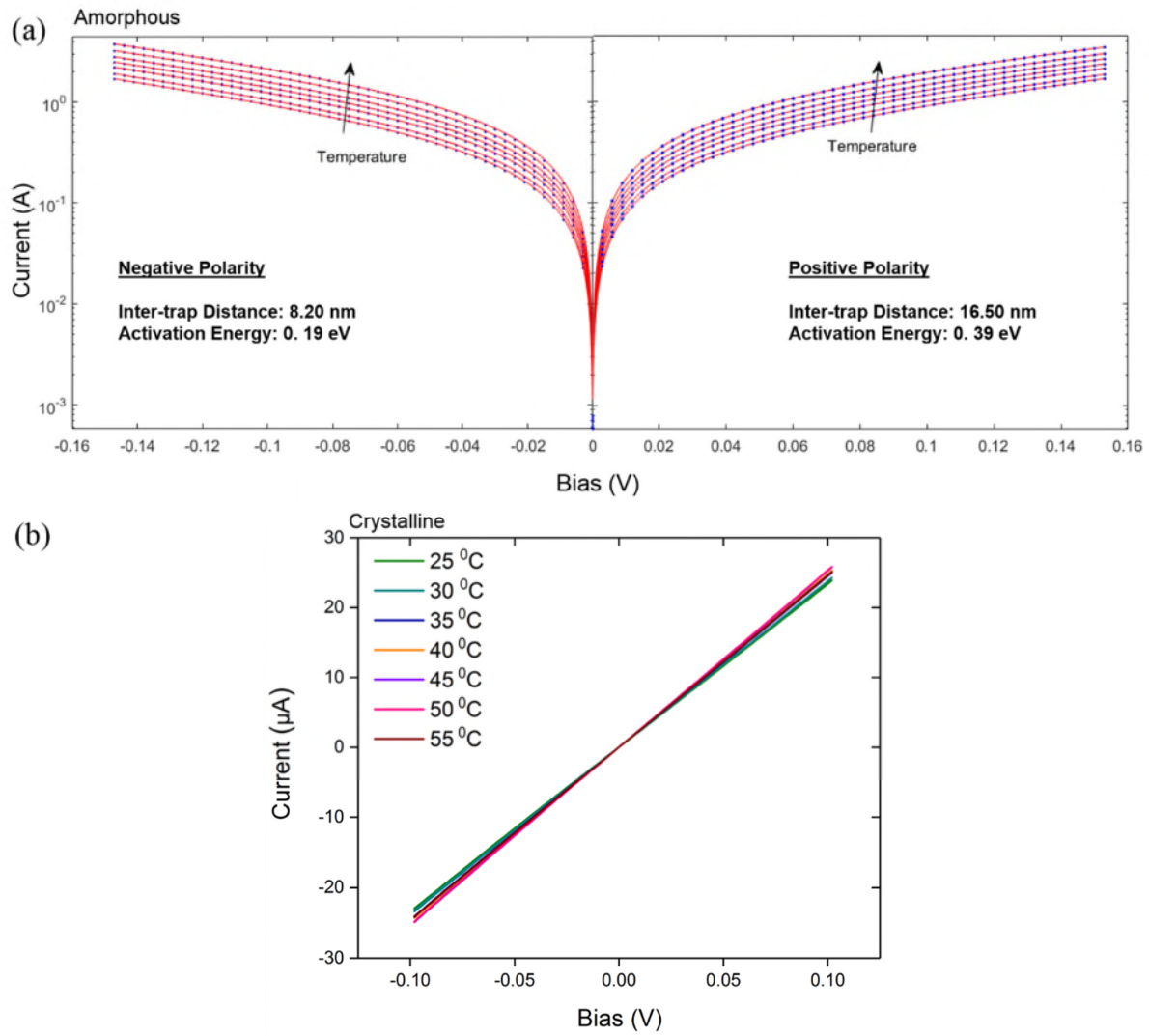


Figure S4. I-V fitting of the amorphous state at various temperatures. (a) The IV data in the amorphous state at temperatures spanning from 30 $^{\circ}$ C to 60 $^{\circ}$ C in increments of 5 $^{\circ}$ C is fitted with the modified Poole-Frenkel model: $I = K' e^{(-\Phi_b/KT)} \sinh((q/KT) \cdot (Vdz/2t))$ where K' is a fitting parameter, K is the Boltzmann constant in eV, Φ_b is the activation energy (energy barrier) in eV, V is the applied voltage in volts, dz is the inter-trap distance and t is the GST thickness. We find that the model cannot fit the IV data for the entire range sweep between -0.1 V to 0.1 V. However the model fits nicely when the IV data is considered for the negative and positive polarities. For the negative polarity, the inter trap distance is calculated 8.20 nm as opposed to 16.50 nm in the positive polarity and similarly the activation energy is found to be 0.2 eV as opposed to 0.4 eV in the positive polarity. This abnormality is indicative of contributions to the IV characteristics from the contacts (schottky barriers). We find that the IVs cannot also be solely fitted with the thermionic model that describes the charge transport in the metal-semiconductor-metal systems, confirming that both the Poole-Frenkel transport

and the thermionic emission in addition to direct tunnelling govern the charge transport characteristics in our devices, and (b) The IV data in the crystalline state at temperatures spanning from 20 °C to 55 °C in increments of 5 °C. The current is found to not linearly increase with temperature, but instead decrease. This is indicative of metallic behaviour in crystalline GST due to its degenerate nature (heavy *p*-doping)

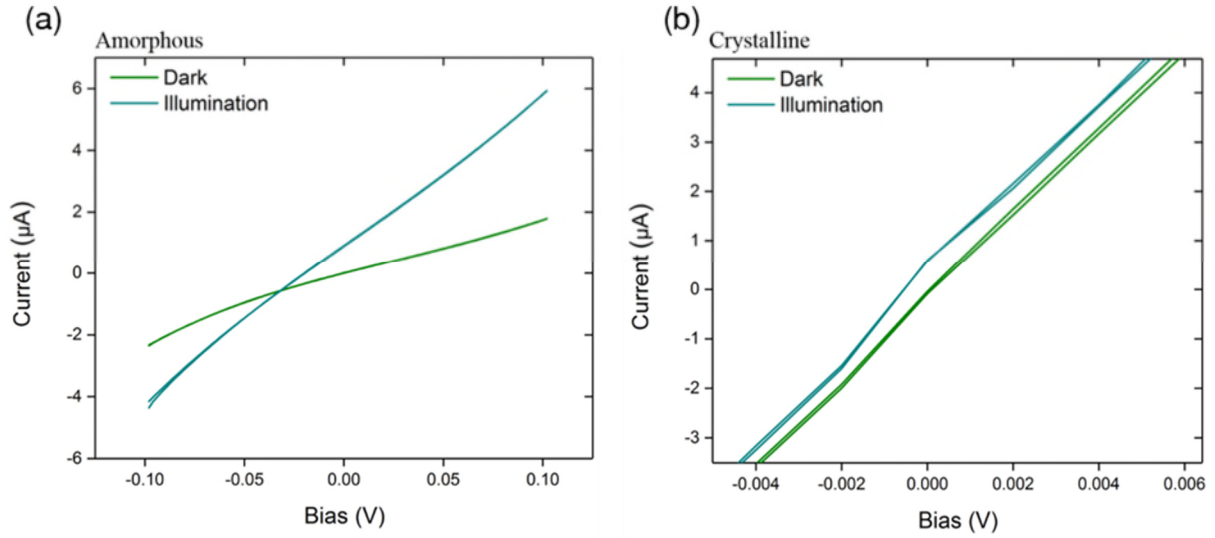


Figure S5. **Photo-behaviour at 1590 nm illumination.** (a) IV characteristics of a 25 μm by 25 μm device (Ta/Pt(50nm)/ITO (40nm)/GST(21nm)/ITO(80nm)) illuminated at 2mW of 1550 nm in the amorphous state of GST, and (b) similar measurements in the crystalline state of GST

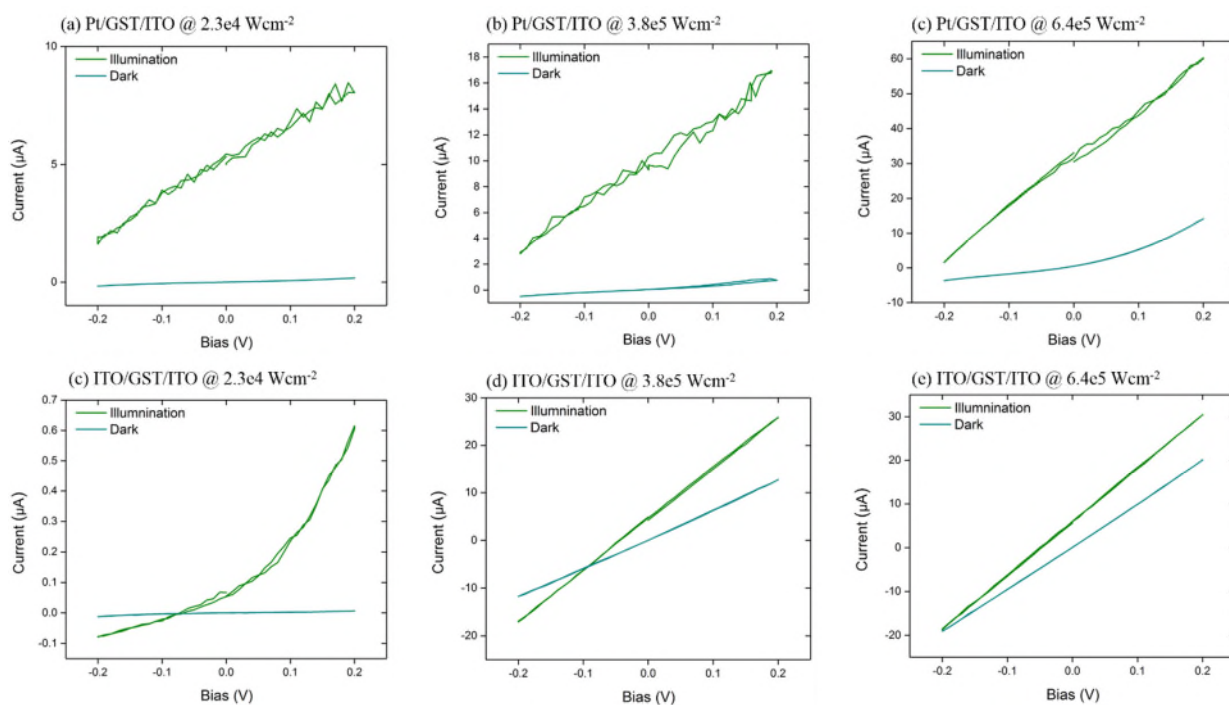


Figure S6. **Photo-behaviour in other micron sized devices.** (a,b,c) IV characteristics of a 1 um by 1 um device ITO (30nm)/GST (15nm)/Pt (7nm) illuminated at 405nm. This device has asymmetric schottky barrier due to differing contacts. The device photo-voltaic and photo-response increases with increasing laser power, and the devices partially crystallize; and (c,d,e) IV characteristics of a 1 um by 1 um device ITO (30nm)/GST (15nm)/ITO (20 nm) illuminated at 405nm. This device has asymmetric schottky barrier due to fabrication induced changes in the contacts. The photo-voltaic and photo-response increases with increasing laser power and the device crystallizes more readily than the before due to decreased thermal losses.

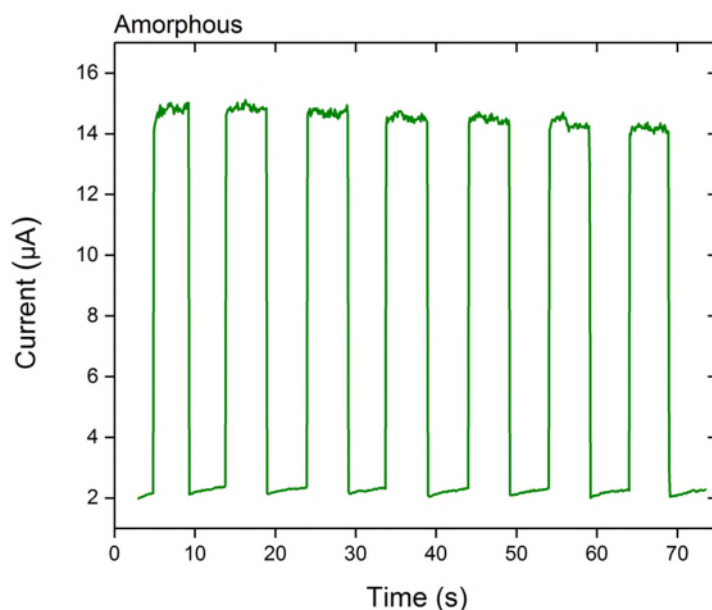


Figure S7. **Photo-stability of $\text{Ge}_{40}\text{Te}_{60}$.** Current vs time characteristics of a device: Ta (10nm)/Pt (50nm)/GeTe (19nm)/65 nm (ITO) under pulsed illumination (1 mW/637nm) in the amorphous state of $\text{Ge}_{40}\text{Te}_{60}$. Note that the dark current is stable after every measurement, which is indicative of absence of phot-structural effects that are understood to alter the dark current. The slight deviation in the photo-current is from the drift in the laser beam away from the sample. We find that GST has a greater photo-response than GeTe, most likely due to differing material chemistry.

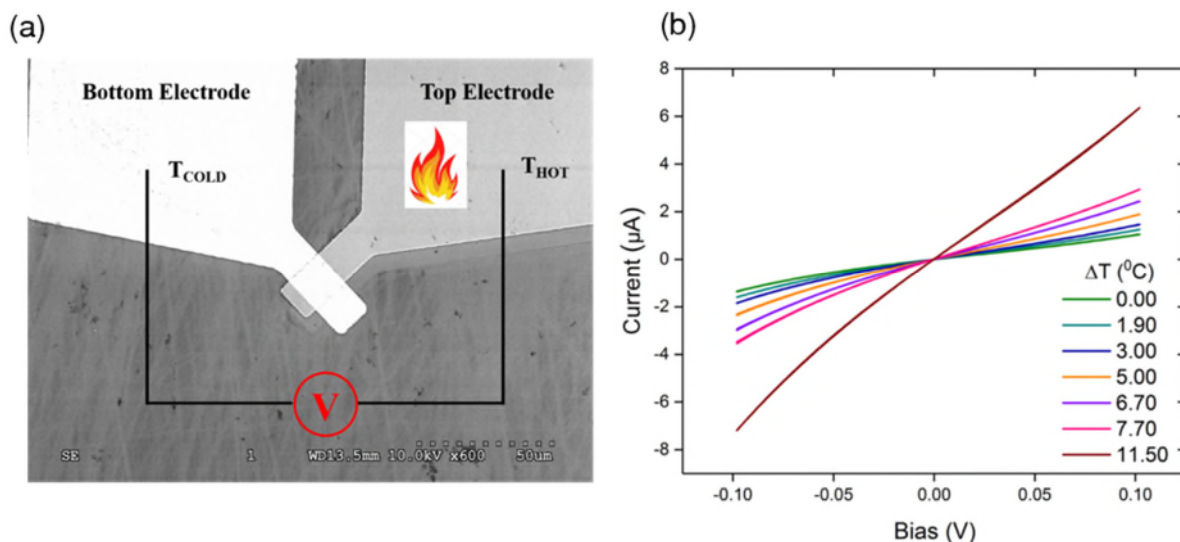


Figure S8. **Thermoelectric effect measurements.** (a) Scanning electron micrograph of device illustrating thermoelectric measurements. The top ITO electrode is preferentially heated to create a temperature difference in order to simulate photo-thermoelectric effects (heating of top ITO electrode from laser illumination); and (b) IV characteristics of the device at various

temperature differences. Note the absence of zero bias short-circuit current as opposed to observed under laser illumination. This indicates that photo-thermoelectric do not dominate the photo-response observed in our devices. Increased current is indicative of thermal activation of charge carriers (see Figure S5).

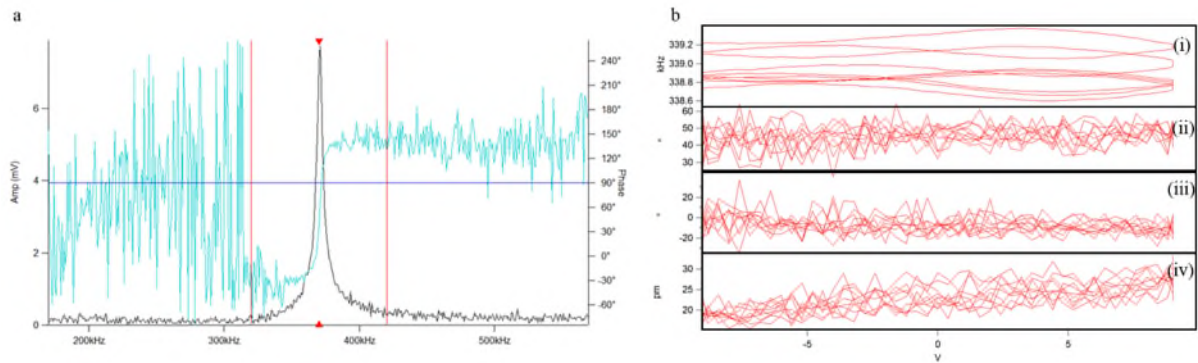


Figure S9. **Ferroelectricity measurements.** (a) Contact Resonance Measurements. An n-doped silicon atomic force microscopy probe is scanned over a range of frequencies on the device (amorphous GST) in the contact-mode operation to determine the resonance frequency (indicative of tip-sample stiffness). (b) Hysteresis loop measurements carried out at the contact resonance frequency to maximize the signal to noise ratio. (i) Five cycles of frequency sweep (forward and reverse), (ii) and (iii) corresponding phase of the probe from deflection. Hysteresis is not observed which is indicative of absence of ferroelectric switching. (iv) Amplitude of the probe deflection. Hysteresis is not observed which is indicative of absence of ferroelectric switching.

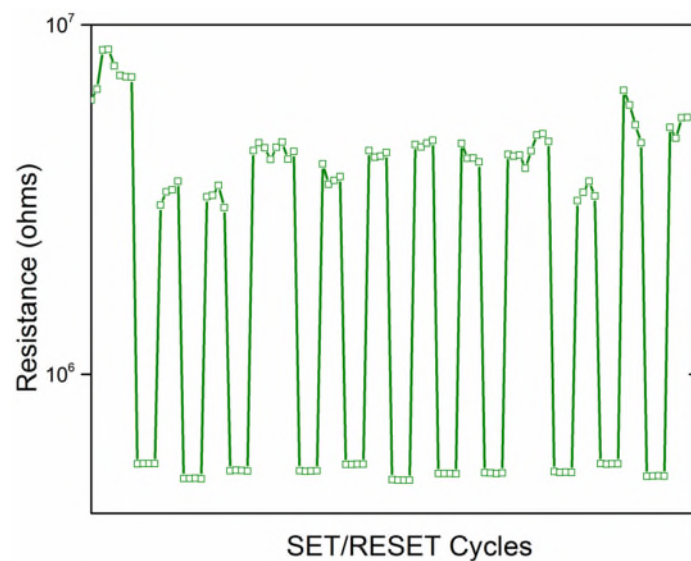


Figure S10. **Cyclic Switching.** A cross bar device (ITO (20nm)/GST(15nm)/ITO(20nm)) with active region 1μm by 1μm crystallized (using standard IVs) and amorphised (4 V, 50 ns Wide,

5 ns rise and fall edge, single pulses) multiple times. An order magnitude change in resistance is observed from phase transformation.

References

- (1) Ríos, C.; Hosseini, P.; Taylor, R. A.; Bhaskaran, H. Color Depth Modulation and Resolution in Phase-Change Material Nanodisplays. *Adv. Mater.* **2016**, 4720–4726.